Solar Phys (2014) 289:503–514
DOI 10.1007/s11207-013-0339-z

A Full-Sun Magnetic Index from Helioseismology Inferences

I. González Hernández · M. Díaz Alfaro · K. Jain · W.K. Tobiska · D.C. Braun · F. Hill · F. Pérez Hernández

Received: 4 October 2012 / Accepted: 28 May 2013 / Published online: 9 July 2013

Abstract Solar magnetic indices are used to model the solar irradiance and ultimately to forecast it. However, the observation of such indices is generally limited to the Earth-facing hemisphere of the Sun. Seismic maps of the far side of the Sun have proven their capability to locate and track medium–large active regions at the non-visible hemisphere. We present here the possibility of using the average signal from these seismic far-side maps, combined with similarly calculated near-side maps, as a proxy to the full-Sun magnetic activity.

Keywords Helioseismology · Magnetic fields · Irradiance forecast

1. Introduction

Photospheric features of solar activity account for a large portion of the total solar irradiance (TSI) variation, with a superimposed modulation due to the solar cycle (Fröhlich, 1993). Magnetic indices related to photospheric activity, such as the Mount Wilson Plage Strength Index (MPSI) and the Mount Wilson Sunspot Index (MWSI: Parker, Ulrich, and Pap, 1998),

Solar Origins of Space Weather and Space Climate
Guest Editors: I. González Hernández, R. Komm, and A. Pevtsov

I. González Hernández (✉) · K. Jain · F. Hill
National Solar Observatory, Tucson, AZ 85719, USA
e-mail: irenegh@nso.edu

M. Díaz Alfaro · F. Pérez Hernández
Instituto de Astrofísica de Canarias, Tenerife 38205, Spain

W.K. Tobiska
Space Environment Technologies, Los Angeles, CA, USA

D.C. Braun
NorthWest Research Associates, Boulder, CO 80301, USA

F. Pérez Hernández
Universidad de la Laguna, Tenerife 38200, Spain

as well as magnetic activity proxies such as the 10.7 cm radio flux ($F_{10.7}$) (Covington, 1969; Kundu, 1965), the Mg II core-to-wing ratio (Viereck *et al.*, 2001) and the Lyman-alpha (Lyα) intensity (Woods *et al.*, 2000) have been traditionally used as input to the modeling and prediction tools for TSI (Tobiska, 2002; Jain and Hasan, 2004) and ultraviolet and extreme ultraviolet (UV/EUV) irradiance (Viereck *et al.*, 2001; Dudok de Wit *et al.*, 2008). However, at each particular point in time, these indices contain information of the magnetic activity only for the solar hemisphere facing the Earth.

The *Solar Wind Anisotropies* (SWAN) instrument, onboard SOHO, has been producing maps of backscattered solar (Lyα) radiation from the interplanetary medium since 1996 (Bertaux *et al.*, 1997). These data are the basis for forecasting several solar indices: $F_{10.7}$, Mg II, and the Lyα intensity (http://swan.projet.latmos.ipsl.fr), proving the potential of using far-side information.

For the last ten years, local helioseismology methods have provided a way to map medium-to-large active regions on the non-visible hemisphere of the Sun using information carried by waves that propagate all the way from the far side to the near side, where these waves are observed (Lindsey and Braun, 2000b; Zhao, 2007). The waves that pass through areas of strong magnetic fields experience a phase shift (Braun *et al.*, 1992) that is measurable when compared with a model representing waves that propagate between two points in the quiet photosphere. Maps of the difference between the model and the measured phase shift present large perturbations in those areas of concentrated magnetic field, such as active regions. Seismic maps calculated using this technique are currently used as another space weather forecasting tool and are available at http://gong.nso.edu/data/farside/ and http://sdo.gsfc.nasa.gov/data.

In this article, we introduce the idea of calculating a magnetic index that accounts for the whole solar surface, the Total Solar Seismic Magnetic Index (TSSMI) from the seismic signature of active regions. The TSSMI is an integrated value over both the observed and the non-visible hemispheres calculated by averaging the seismic signal (phase shift or travel-time difference) produced by surface magnetic activity, namely sunspots and plages, on the waves. This index is a proxy to the photospheric magnetic activity over the whole Sun and could be used to research long-term variations of the Sun without the limitations of the near-side-only observations. Furthermore, the far-side component of this index (Far Side Seismic Magnetic Index, FSSMI) can be used as input to solar irradiance forecast models.

2. Data Analysis

To compute the seismic index, we use near-side and far-side maps for the period of January 2002 to December 2005. The maps are calculated using the phase-sensitive seismic-holography technique as described by Lindsey and Braun (2000a) and Braun and Lindsey (2001). The technique is based on the comparison between the travel path determined for observed waves (as velocity field perturbations in the solar photosphere) compared with a model of the quiet Sun (Green's functions) for each location of the solar surface. When waves travel though an area of concentrated magnetic fields, they accelerate (Braun *et al.*, 1992), producing a phase shift with respect to the model. Hence, the seismic-holography maps show areas of large phase shift, which are interpreted as active regions.

Each far-side synoptic map is computed from a one-day series of 1440 *Global Oscillation Network Group* (GONG) Dopplergrams with a cadence of 60 s. If there are missing observations, the gaps are zero-filled. The Dopplergrams are taken in the photospheric line Ni I λ 6768 Å and have a spatial resolution of ≈ 5 arcsec (Harvey *et al.*, 1996). Each Dopplergram is Postel projected into a 200 $\times$ 200-pixel map. The maps are then stacked into a

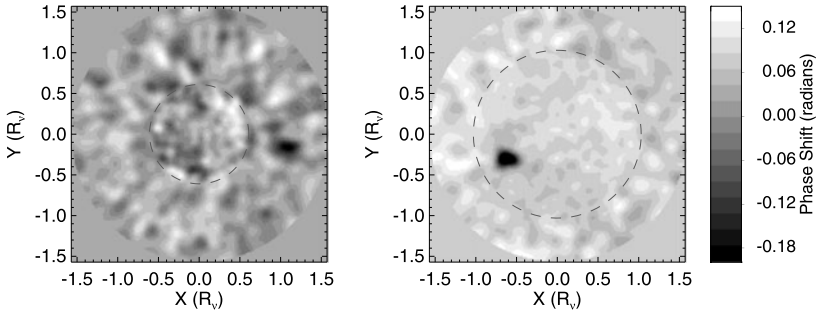

Figure 1 Left panel: Postel projection of the far-side map of the phase shift for 5 September 2005 showing the strong seismic signature of active region NOAA 10808 two days before it appeared at the east limb. Right panel: Postel projection of the helioseismic near-side map showing the same active region on 11 September 2005. The dotted line represents the center of the merged region which is different for the near- and far-side maps.

1440-frame datacube to which the technique as described by Lindsey and Braun (2000a) is applied. The resulting far-side image is itself a Postel projection. To reduce the errors in the calibration, only maps calculated from series with a clear-weather duty cycle greater than 80 % have been considered.

Because of geometrical limitations of the near-side observation area (pupil) combined with variable sensitivity with disk position, helioseismic-holography maps of the far side have been traditionally calculated in two parts: the central area, using the correlation between waves that bounce once at the surface (2-skip) before reaching the observation point, and the peripheral area, using the correlation between waves that do not bounce (1-skip) and bounce twice (3-skip) (Braun and Lindsey, 2001). During this research, we have followed this schema when calculating the far-side maps.

Different seismic imaging techniques have been used to create 3D structural and dynamic maps of active regions in the near side of the Sun for some time (*e.g.* Chou, 2000; Ilonidis, Zhao, and Kosovichev, 2012). They use shorter ray paths that provide more resolution and a plane-parallel approximation to reduce the computer load, but this approach allows only for small areas to be analyzed. For this work, we have created full-Sun maps by extending the same seismic-holography technique that computes the far-side to cover also the near-side. To keep consistency with the far-side calculations, we use waves following long ray paths and spherical geometry computations. Because of the geometrical limitations of the observational pupils, the near-side has been calculated also in two parts: the central part using 1×1-skip ray-path correlations, and the peripheral area, using 1×3-skip correlations. Mapping the observed side with a similar schema allows us to merge the front- and far-side inferences into a single full-Sun map that will be the basis for the calculation of the seismic magnetic index.

Figure 1 shows two seismic maps in Postel projection. The left panel presents the Postel projection of the far-side map of phase shift for 5 September 2005, showing the strong seismic signature of active region NOAA 10808 two days before it appeared at the east limb. The right panel is the corresponding Postel projection of the helioseismic near-side map, showing the same active region on 11 September 2005. Dark areas in the map correspond to negative phase signatures introduced by magnetic regions. The apparent difference in the latitudinal location of the active region in both maps is due to the B_0 angle (the angle of inclination of the solar equator on the ecliptic) being extreme during that period, which appears as a displacement in the y-coordinate in these Postel projected maps centered on

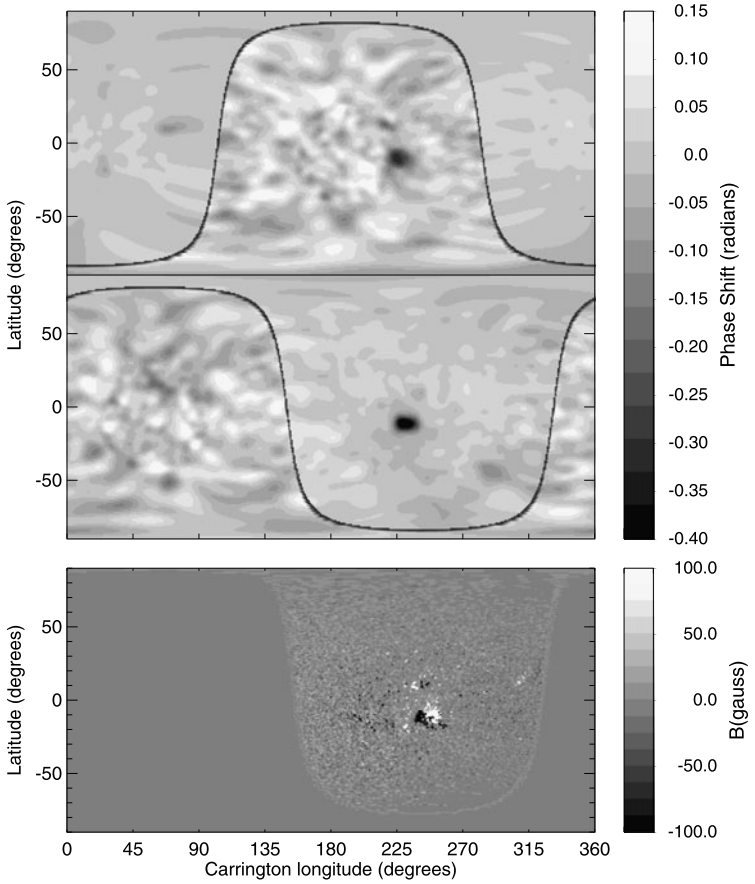

Figure 2 Longitude–latitude projection of the combined front–far side calculation into full-Sun maps. Top: 3 September 2005 map showing active region NOAA 10808. Middle: 13 September 2005 map of the same active region in the front side. Bottom: Longitude–latitude projection of the MDI magnetogram for 13 September 2005, showing the same active region as observed by this instrument onboard SOHO.

disk center. Because we use similar waves for the analysis, the resolution on both maps is similar. However, since the near-side map consist largely of 1×1-skip correlations, the noise is smaller. This is due to the dispersion that waves undergo when bouncing at the surface: the less bounces, the less noisy the results are. The dashed lines represent the separation between the central and the peripheral areas calculated using different wave combinations for each of the maps.

The near-side and far-side separated maps are then re-projected into a longitude–latitude grid and combined into a single map of the full Sun. Examples of full-Sun longitude–latitude projected maps are presented in Figure 2. Far-side and near-side areas are delimited by a dark line. The figures correspond to maps of the same region as in Figure 1 (NOAA 10808) but on different days, 3 September 2005 (top) and 13 September 2005 (middle). The bottom panel is a longitude-latitude projection of the *Michelson Doppler Imager* (MDI: Scherrer *et al.*, 1995) magnetogram for 13 September 2005, showing the same active region as observed by this instrument onboard SOHO.

3. A Near-Side Seismic Magnetic Index (NSSMI)

For validation purposes, we start calculating a near-side seismic index using only the near-side seismic maps. That way we can compare with the standard indices from the observable side of the Sun. The NSSMI is an average over the seismic signal (phase shift) of the near-side maps. We have arbitrarily ignored the positive phase shift in the maps and integrated only over negative values, associated with magnetic features. In addition, we integrate the value of the maps only from -40 to $+40$ degrees latitude, to avoid the noisier latitudes. The seismic far-side maps have been shown to be affected by a solar cycle variation, similar to the superimposed cycle modulation found in TSI measurements. In the case of the seismic maps, this cycle modulation has been associated to either global or localized structural changes in the solar convection zone (González Hernández, Scherrer, and Hill, 2009). To remove this variation each individual map (both near and far side) is corrected by removing a 60-day trailing average.

Figure 3 shows simultaneous values of the composite Lyα index from the Laboratory for Atmospheric and Space Physics (lasp.colorado.edu/lisird/tss), the calculated Mount Wilson sunspot (MWSI) and plage (MPSI) indices (www.astro.ucla.edu), the observed $F_{10.7}$ (www.ngdc.noaa.gov) and Mg II (www.swpc.noaa.gov/ftpmenu/sbuv.html) and the calculated NSSMI from the seismic-holography maps. The sequence spans from January 2002 to December 2005. Figure 4 presents a running mean of 10 days for both the seismic index and the standard solar indices to aid the comparison. A large increase in all of them can be seen associated with the large active regions that produced the Halloween flares at the end of 2003. The different indices have a marked correlation. The Pearson correlation coefficients between each of the traditional ones and the newly calculated seismic index can be found in Table 1 for both the one-day values and the ten-day smoothed series. The corresponding scatter plots are presented in Figure 5.

4. The Total Solar Seismic Magnetic Index (TSSMI)

To complete the full-Sun magnetic index, we follow the same procedure as described in the previous section but using the far-side helioseismic maps to calculate the far-side seismic magnetic index (FSSMI). Finally, we combine the two of them into the total solar seismic magnetic index (TSSMI). Figure 6 presents the three series, near-, far-side, and full-Sun indices.

The 27-day modulation due to the solar rotation is seen in both the near-side index and the far-side one. Two particular scenarios have been highlighted in the figure. Scenario A shows an increase of the integrated phase shift first on the front side index and then in the far side. The solid and dashed lines are plotted 14 days apart, to account for about half solar rotation. Scenario B is the reverse case, when we first have an increase in the far side that then moves to the front side. These are typical cases of active regions emerging in one of the hemispheres (front or far) and moving to the other one. In Scenario A, the active regions live long enough to come back to the front side a second time. The time lag between the near-side index and the far-side one is determined by the solar rotation, as the active regions move from the front to the far side of the Sun and *vice versa*. However, since active regions emerge and decay in a semi-random manner on both the front and far side of the Sun, trying to find a correlation between the two data sets to infer a time lag is not trivial, since it will be positive for certain periods, negative for others, and a complex mix for periods of high activity. The 27-day modulation still shows a residual in the full-Sun index, which is most probably due

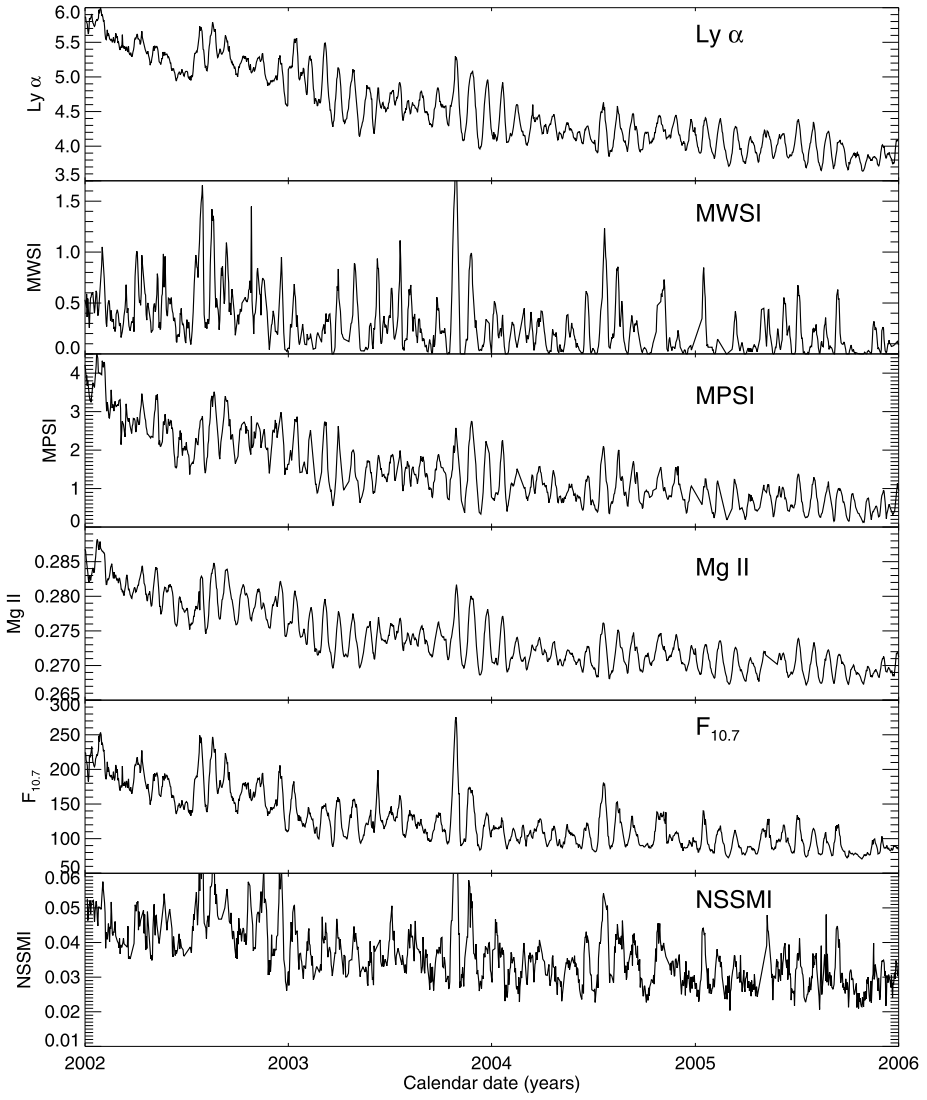

Figure 3 Simultaneous observations/calculations of the Lyα composite index, the Mount Wilson sunspot and plage indices, Mg II, $F_{10.7}$ and the near-side seismic magnetic index. The sequence spans from January 2002 to December 2005. The sign of the seismic magnetic index has been inverted to aid the comparison. The units of the different indices are: solar flux units for $F_{10.7}$, 10^{11} photons $cm^{-2}\,s^{-1}$ for Lyα, Gauss for the MPSI and MWSI and radians for the NSSMI.

to a combination of the location-dependent sensitivity of the helioseismic maps and the fact that the front- and far-side indices have been calculated using a different combination of waves, which introduces a phase difference between the two inferences.

Although the far-side maps are noisier than the near-side ones, the ten-day smooth indices obtained from both series seem to present a similar behavior and background, but with a positive phase shift for the FSSMI. For the purpose of this article, we have simply added

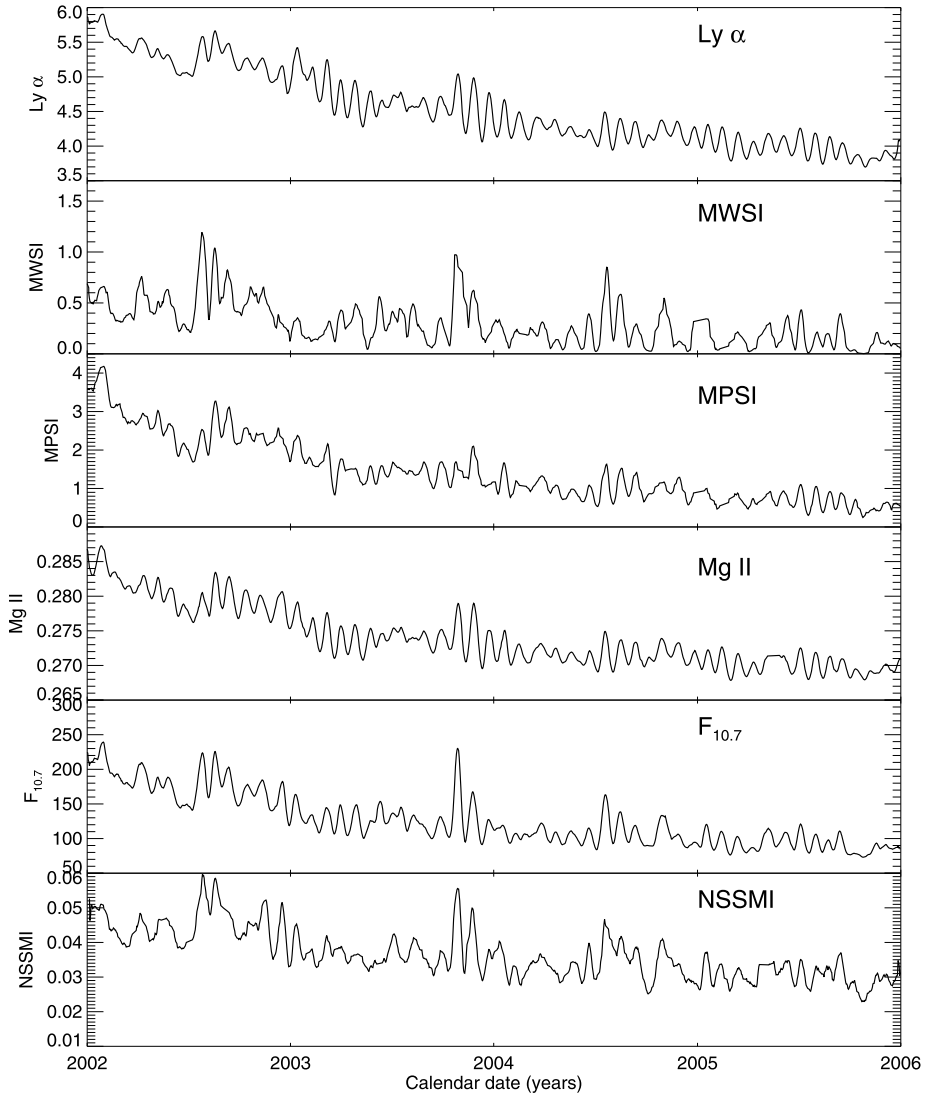

Figure 4 Ten-day smoothed averages of the simultaneous observations/calculations of the Lyα composite index, the Mount Wilson sunspot and plage indices, Mg II, $F_{10.7}$ and the near-side seismic magnetic index. The sequence spans from January 2002 to December 2005. The sign of the seismic magnetic index has been inverted to aid the comparison.

the near-side and the far-side values to compute the TSSMI. But the shift between the far-side and the near-side maps needs to be investigated, before the index is used as a proxy. A possible explanation comes from the empirical correction of the phase shift due to the superadiabatic layers at the near surface (Lindsey and Braun, 2000a). The different parts of the maps use waves which follow 1-skip, 2-skip or 3-skip paths, that is, they do not bounce, bounce one or twice before reaching the observation area; if the phase shift correction is not ideal, the different parts of the map will be affected differently.

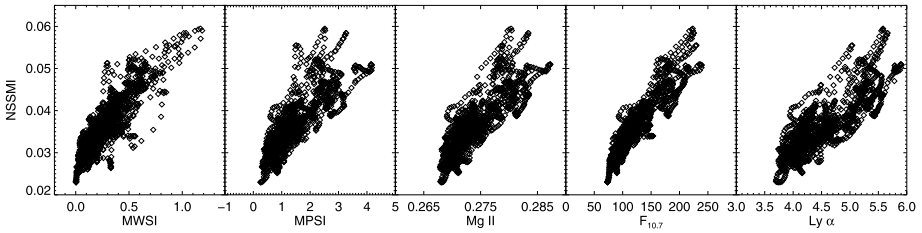

Figure 5 Scatter plots of the ten-day average NSSMI and each of the other front-side magnetic indices. A strong linear correlation can be observed in most of them, with the largest corresponding to that of $F_{10.7}$. The Pearson correlation coefficients are presented in Table 1.

Table 1 Pearson correlation coefficient between each of the standard front-side magnetic indices and the new seismic index.

Index	Correlation coeff. One-day values	Correlation coeff. Ten-day smoothed avg.
MWSI	0.86	0.87
MPSI	0.78	0.82
Mg II	0.79	0.84
$F_{10.7}$	0.89	0.92
Lyα	0.77	0.84

5. Discussion and Future Work

The comparison between the NSSMI and the standard near-side indices (see Figures 3, 4, and Table 1) shows the capability of seismic inferences to provide a new proxy for the solar magnetic activity. The helioseismology technique used to calculate far-side maps of the Sun, as well as the near-side maps calculated for this particular research, use waves that propagate following long ray paths. The sensitivity of such waves to small active regions is limited. This is due to the small perturbation that these active regions introduce in the wave propagation and the limited spatial resolution of the waves used in the analysis.

In general, we expect to find a larger correlation between the NSSMI and those indices that are sensitive to large, strong magnetic areas in the photosphere. The MPSI and the MWSI are calculated as the sum of the number of pixels with magnetic field intensity between 10 and 100 Gauss and larger than 100 Gauss and then divided by the total of number of pixels in the magnetogram (regardless of magnetic field strength), respectively. These are proxies of the strong photospheric magnetic fields, which are the main contributors to the phase shift of seismic inferences. Hence, we expect these indices to be closer to the NSSMI. The correlation with these two indices is high, however, we find a larger correlation with the $F_{10.7}$ index, which is the integrated emission from the solar disc at 2.8 GHz, *i.e.*, 10.7 cm wavelength, and serves as a proxy for the solar EUV emission. It mainly represents the contributions from sunspots and radio plages in the upper chromosphere in addition to the quiet-Sun background emission (Covington, 1969; Kundu, 1965).

A very strong correlation is also found with another chromospheric-related index, the Mg II. The Mg II core-to-wing ratio is derived by taking the ratio of the h and k lines of the solar Mg II feature at 280 nm to the background or wings at approximately 278 nm and 282 nm. The h and k lines are variable chromospheric emissions while the background

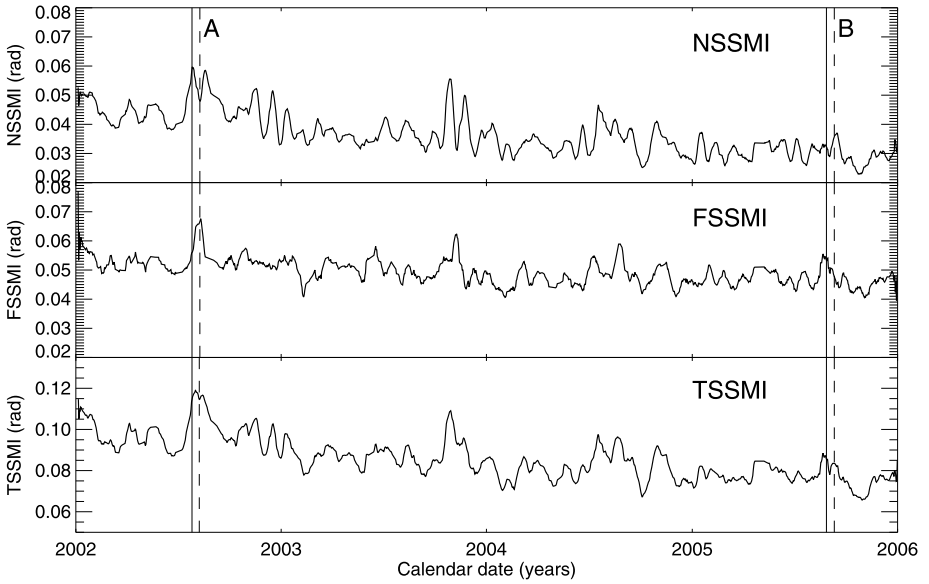

Figure 6 Values of the calculated near-side seismic magnetic index, the far-side seismic magnetic index and the combination of both into the total solar seismic magnetic index. The sequence spans from January 2002 to December 2005. A and B represents two scenarios where the index increases first in the near side and then in far side and *vice versa*, respectively.

emissions are more stable. This ratio seems to be a robust measure of chromospheric activity, mainly for solar UV and EUV emissions (Viereck *et al.*, 2001). At this point, we cannot explain these results, particularly given the fact that the quiet-Sun variation has been removed from the seismic maps; however, it provides the possibility of intercalibration between the near-side EUV indices and the seismic index. An in-depth comparison with longer series and filtering different areas of the seismic maps could help understand these results. The actual physical mechanism that produces the phase shift in the observed waves when they propagate through a strong magnetic field is still under investigation.

Finally, the correlation with the composite Lyα index is also reasonable given that Lyα emission serves as the best proxy for the irradiance originated from the transition region (Woods *et al.*, 2000; DeLand and Cebula, 2008).

In all cases, center-to-limb effects in the different standard proxies, combined with the location-dependent sensitivity of the seismic inferences, can contribute to lower the correlation. In fact, there may be an anticorrelation component with the emission-based proxies, since those incorporate a higher contribution of magnetic activity towards the limb, while the helioseismology inferences present stronger signatures close to disk center. New sets of artificial helioseismology data are currently available, which can be analyzed from different vantage points and will help to understand (and possibly correct for) the sensitivity function on the seismic maps.

The real potential of the seismic inferences is the ability to provide an index that comprises both the Earth-facing and the non-visible hemisphere solar magnetic activity (see Figure 6). The validation of the NSSMI *versus* the near-side indices means that the FSSMI, calculated with a very similar approach, provides useful information from an integrated perspective. The FSSMI contains information of the surface magnetic activity that will be

facing Earth days in advance. In theory, solar models that use the integrated near-side indices as input to their calculations could use data provided by the far-side integrated index that would be facing Earth at a given time; so, if a far-side event is occurring, the Earth-facing part of the disk in, say six days, would be the relevant proxy for the six-day forecast. The part of the far-side disk that would be Earth-facing in ten-days would be the ten-day forecast and so on. It has been shown that short-term forecasting of UV irradiance can be improved when adding far-side seismic maps (Fontenla *et al.*, 2009). We expect that the integrated far-side seismic magnetic index will also help to complement the near-side indices for more accurate forecasting of the solar irradiance.

The TSSMI can be used for long-term studies of solar variability. The GONG project has been operating for almost 18 years, providing the capability of calculating the full-Sun seismic index for more than one solar cycle. So far, long-term studies of solar variability have been biased by the limitation of having only near-side observations. A comparison between long-term variation of the TSSMI and the standard near-side indices could provide insight as to have good the near-side indices have been at reproducing the full-Sun long-term variations. Any new knowledge in that respect will help to constrain the solar dynamo models. González Hernández, Scherrer, and Hill (2009) showed a variation of the wave propagation times through the solar interior that was highly correlated with the solar cycle, using integrated values of far-side seismic maps. We intend now to use the full-Sun approach to repeat the experiment, in an attempt to further understand the global *versus* local nature of the cycle dependence.

As stated before, the current seismic-holography method to calculate far-side and near-side maps using large ray paths has its limitations. So far, the technique is sensitive mainly to the contributions of medium-to-large size active regions. Two approaches are being investigated to improve the method, so it can account also for smaller active regions. The model used in helioseismic holography is being improved. Pérez Hernández and González Hernández (2010) developed a formalism that gives a more accurate representation of the wave field in the quiet Sun. Their preliminary results show a computational advantage in using these new Green's functions, as well as an increase of the signal to noise of ~ 30 %. In addition, employing the 2×3-skip correlation seems to further increase the signal to noise in far-side seismic maps calculated using the time–distance technique (Zhao, 2007), we are currently exploring this possibility for seismic holography.

Future work includes the calibration of the full-Sun seismic magnetic index in terms of other solar indices/proxies like $F_{10.7}$, Mg II, and Lyα which, in turn, can be used as input to models such as the Jacchia–Bowman 2008 (JB2008; Bowman *et al.*, 2008) thermospheric density model used primarily for low Earth orbiting satellite drag calculations. No doubt other models that need full-Sun information will benefit from including different far-side data. The *Solar TErrestrial RElations Observatory* (STEREO) EUV images have been used to quantify the reliability of the seismic far-side maps (Liewer *et al.*, 2012), so integrated quantities from STEREO observations can also be used to validate the seismic index.

Acknowledgements The authors thank C. Lindsey for his extensive contribution to the NISP/GONG far-side pipeline and A. Malanushenko for the customization of part of the code. This work utilizes GONG data obtained by the NSO Integrated Synoptic Program (NISP), managed by the National Solar Observatory, which is operated by the Association of Universities for Research in Astronomy (AURA), Inc. under a cooperative agreement with the National Science Foundation. The data were acquired by instruments operated by the Big Bear Solar Observatory, High Altitude Observatory, Learmonth Solar Observatory, Udaipur Solar Observatory, Instituto de Astrofísica de Canarias, and Cerro Tololo Interamerican Observatory. SOHO is a project of international cooperation between ESA and NASA. This study includes data from the synoptic program at the 150-Foot Solar Tower of the Mt. Wilson Observatory. The Mt. Wilson 150-Foot Solar Tower

is operated by UCLA, with funding from NASA, ONR, and NSF, under agreement with the Mt. Wilson Institute. We thank NOAA for the availability of the Mg II and $F_{10.7}$ data and LASP for the composite Lyα index. Part of the research has been supported by NASA grant NNH1AQ24I. Part of this work was supported by the Spanish National Research Plan under project AYA2010-17803.

References

Bertaux, J.L., Quémerais, E., Lallement, R., Kyrölä, E., Schmidt, W., Summanen, T., Goutail, J.P., Berthé, M., Costa, J., Holzer, T.: 1997, First results from SWAN Lyman-α solar wind mapper on SOHO. *Solar Phys.* **175**, 737. ADS:1997SoPh..175..737B, doi:10.1023/A:1004979605559.

Bowman, B.R., Tobiska, W.K., Marcos, F., Huang, C.: 2008, The thermospheric density model JB2008 using new EUV solar and geomagnetic indices. In: *37th COSPAR Scientific Assembly*, **37**, 367.

Braun, D.C., Lindsey, C.: 2001, Seismic imaging of the far hemisphere of the Sun. *Astrophys. J. Lett.* **560**, L189. ADS:2001ApJ...560L.189B, doi:10.1086/324323.

Braun, D.C., Duvall, J.T.L., Labonte, B.J., Jefferies, S.M., Harvey, J.W., Pomerantz, M.A.: 1992, Scattering of p-modes by a sunspot. *Astrophys. J.* **391**, 113. ADS:1992ApJ...391L.113B. doi:10.1086/186410.

Chou, D.-Y.: 2000, Acoustic imaging of solar active regions (Invited Review). *Solar Phys.* **192**, 241. ADS:2000SoPh..192..241C.

Covington, A.E.: 1969, Solar radio emission at 10.7 cm, 1947 – 1968. *J. Roy. Astron. Soc. Can.* **63**, 125. ADS:1969JRASC..63..125C.

DeLand, M.T., Cebula, R.P.: 2008, Creation of a composite solar ultraviolet irradiance data set. *J. Geophys. Res.* **113**, A11103. ADS:2008JGRA..11311103D, doi:10.1029/2008JA013401.

Dudok de Wit, T., Kretzschmar, M., Aboudarham, J., Amblard, P.-O., Auchère, F., Lilensten, J.: 2008, Which solar EUV indices are best for reconstructing the solar EUV irradiance? *Adv. Space Res.* **42**, 903. ADS:2008AdSpR..42..903D, doi:10.1016/j.asr.2007.04.019.

Fontenla, J.M., Quémerais, E., González Hernández, I., Lindsey, C., Haberreiter, M.: 2009, Solar irradiance forecast and far-side imaging. *Adv. Space Res.* **44**, 457. ADS:2009AdSpR..44..457F, doi:10.1016/j.asr.2009.04.010.

Fröhlich, C.: 1993, Relationship between solar activity and luminosity. *Adv. Space Res.* **13**, 429. ADS:1993AdSpR..13..429F, doi:10.1016/0273-1177(93)90515-D.

González Hernández, I., Scherrer, P., Hill, F.: 2009, A new way to infer variations of the seismic solar radius. *Astrophys. J. Lett.* **691**, L87. ADS:2009ApJ...691L..87G, doi:10.1088/0004-637X/691/2/L87.

Harvey, J.W., Hill, F., Hubbard, R.P., Kennedy, J.R., Leibacher, J.W., Pintar, J.A., Gilman, P.A., Noyes, R.W., Title, A.M., Toomre, J., Ulrich, R.K., Bhatnagar, A., Kennewell, J.A., Marquette, W., Patron, J., Saa, O., Yasukawa, E.: 1996, The Global Oscillation Network Group (GONG) project. *Science* **272**, 1284. ADS:1996Sci...272.1284H, doi:10.1126/science.272.5266.1284.

Ilonidis, S., Zhao, J., Kosovichev, A.: 2012, Detection of emerging sunspot regions in the solar interior. *Science* **333**, 993. ADS:2012Sci...336..296I, doi:10.1126/science.1215539.

Jain, K., Hasan, S.S.: 2004, Modulation in the solar irradiance due to surface magnetism during cycles 21, 22 and 23. *Astron. Astrophys.* **425**, 301. ADS:2004A&A...425..301J, doi:10.1051/0004-6361:20047102.

Kundu, M.R.: 1965, *Solar Radio Astronomy*, Interscience, New York.

Liewer, P.C., González Hernández, I., Hall, J.R., Thompson, W.T., Misrak, A.: 2012, Comparison of far-side STEREO observations of solar activity and active region predictions from GONG. *Solar Phys.* **281**, 3. ADS:2012SoPh..281....3L, doi:10.1007/s11207-012-9932-9.

Lindsey, C., Braun, D.C.: 2000a, Basic principles of solar acoustic holography (Invited Review). *Solar Phys.* **92**, 261. ADS:2000Sci...287.1799L, doi:10.1126/science.287.5459.1799.

Lindsey, C., Braun, D.C.: 2000b, Seismic images of the far side of the Sun. *Science* **287**, 1799. ADS:2000SoPh..192..261L.

Parker, D.G., Ulrich, R.K., Pap, J.M.: 1998, Modeling solar UV variations using Mount Wilson Observatory indices. *Solar Phys.* **177**, 229. ADS:1998SoPh..177..229P.

Pérez Hernández, F., González Hernández, I.: 2010, Green's functions for far-side seismic images: a polar-expansion approach. *Astrophys. J.* **711**, 853. ADS:2010ApJ...711..853P, doi:10.1088/0004-637X/711/2/853.

Scherrer, P.H., Bogart, R.S., Bush, R.I., Hoeksema, J.T., Kosovichev, A.G., Schou, J., Rosenberg, W., Springer, L., Tarbell, T.D., Title, A., Wolfson, C.J., Zayer, I., MDI Engineering Team: 1995, The solar oscillations investigation – Michelson Doppler Imager. *Solar Phys.* **162**, 129. ADS:1995SoPh..162..129S. doi:10.1007/BF00733429.

Tobiska, W.K.: 2002, Variability in the solar constant from irradiances shortward of Lyman-alpha. *Adv. Space Res.* **29**, 1969. ADS:2002AdSpR..29.1969T, doi:10.1016/S0273-1177(02)00243-0.

Viereck, R., Puga, L., McMullin, D., Judge, D., Weber, M., Tobiska, W.K.: 2001, The Mg II index: a proxy for solar EUV. *Geophys. Res. Lett.* **28**, 1343. ADS:2001GeoRL..28.1343V, doi:10.1029/2000GL012551.

Woods, T.N., Tobiska, W.K., Rottman, G.J., Worden, J.R.: 2000, Improved solar Lyman-alpha irradiance modeling from 1947 through 1999 based on UARS observations. *J. Geophys. Res.* **105**, 27. ADS:2000JGR...10527195W, doi:10.1029/2000JA000051.

Zhao, J.: 2007, Time–distance imaging of solar far-side active regions. *Astrophys. J. Lett.* **664**, L113. ADS:2007ApJ...664L.139Z, doi:10.1086/520837.